energies

MDPI

Article

Joint Optimization Scheduling of Electric Vehicles and Electro–Olefin–Hydrogen Electromagnetic Energy Supply Device for Wind–Solar Integration

Shumin Sun [1], Chenglong Wang [1], Yan Cheng [1], Shibo Wang [1], Chengfu Wang [2,*], Xianwen Lu [2], Liqun Sun [1], Guangqi Zhou [1] and Nan Wang [1]

[1] Electric Power Research Institute of State Grid Shandong Electric Power Company, Jinan 250003, China
[2] School of Electrical Engineering, Shandong University, Jinan 250061, China
* Correspondence: wangcf@sdu.edu.cn

Abstract

In northern China, the long winter heating period is accompanied by severe wind curtailment. To address this issue, a joint optimization scheduling strategy of electric vehicles (EVs) and electro–olefin–hydrogen electromagnetic energy supply device (EHED) is proposed to promote deep wind–solar integration. Firstly, the feasibility analysis of EVs participating in scheduling is conducted, and the operation models of dispatchable EVs and thermal energy storage EHEDs within the scheduling period are established. Secondly, a control strategy for the joint optimization scheduling of wind–solar farms, EVs, EHEDs, and power grid is constructed. Then, an economic dispatch model for joint optimization of EVs and EHEDs is established to minimize the system operation cost within the scheduling period, and the deep wind–solar integration of the joint optimization model is studied by considering EVs under different demand responses. Finally, the proposed model is solved by CPLEX solver. The simulation results show that the established joint optimization economic dispatch model of EV-EHEDs can improve the enthusiasm of dispatchable EVs to participate in deep wind–solar integration, reduce wind curtailment power, and decrease the overall system operation cost.

Keywords: electro-olefin-hydrogen electromagnetic energy supply; deep wind-solar integration; electric vehicle; joint dispatch model

check for updates

Academic Editor: Kaveh Khalilpour

Received: 29 September 2025
Revised: 27 October 2025
Accepted: 31 October 2025
Published: 10 November 2025

Citation: Sun, S.; Wang, C.; Cheng, Y.; Wang, S.; Wang, C.; Lu, X.; Sun, L.; Zhou, G.; Wang, N. Joint Optimization Scheduling of Electric Vehicles and Electro–Olefin–Hydrogen Electromagnetic Energy Supply Device for Wind–Solar Integration. *Energies* **2025**, *18*, 5911. https://doi.org/10.3390/en18225911

Copyright: © 2025 by the authors. Licensee MDPI, Basel, Switzerland. This article is an open access article distributed under the terms and conditions of the Creative Commons Attribution (CC BY) license (https://creativecommons.org/licenses/by/4.0/).

1. Introduction

1.1. Background and Challenges of the Problem

In recent years, wind and solar power generation have become the most widely promoted and rapidly developed clean energy sources due to their advantages of low environmental impact, wide distribution, and renewability [1,2]. However, influenced by the specific geographic features of northern China, the development of wind and solar power faces the prominent problem of "supply exceeding demand". Additionally, the long heating period and long-term reliance on primary energy sources such as coal for heating have led to prominent issues including energy shortages and environmental pollution. Data from the National Energy Administration shows that the winter wind and solar curtailment in the three northern provinces (Heilongjiang, Jilin, and Liaoning) reached 12 billion kWh in 2023, equivalent to the energy waste of 4 million tons of standard coal, accompanied by approximately 10 million tons of CO_2 emissions [3]. Therefore, how to

adopt reasonable and effective measures to increase wind–solar integration and reduce wind and solar curtailment have become hot issues of social concern [4].

1.2. Research Motivation and Existing Shortcomings

To address the aforementioned issues, the government has introduced policies such as "coal-to-electricity conversion" to promote renewable energy heating and foster the development of a clean and low-carbon society [5–7]. Utilizing wind and solar energy for heating can effectively reduce the curtailment rates of wind and solar power, minimize primary energy consumption, and mitigate environmental pollution. In existing research, the study [8] established a joint optimization scheduling model for wind power and thermal energy storage-based electromagnetic heating equipment, and the study [9] proposed a coordinated heating model incorporating photovoltaic power consumption to minimize daily operational costs. In terms of electric vehicles, the study [10] introduced price-based and incentive-based demand response models to guide orderly charging, and the study [11] developed a two-level optimization model for the coordinated scheduling of wind farms and electric vehicles. Additionally, the study [12] categorized electric vehicle users into three types—"rigid charging," "flexible charging," and "vehicle-to-grid interaction"—of simulated charging demand based on a Poisson process, and proposed an orderly charging strategy under time-of-use pricing, achieving a 5–8% wind power curtailment reduction; the study [13] introduced a battery health cost function and enhanced reverse charging efficiency by 12% through a dynamic compensation mechanism; the study [14] designed a "wind power forecasting-electric vehicle cluster control" two-level framework, employing model predictive control to enable real-time adjustment of charging and discharging power, raising wind power curtailment absorption to 18%; and the study [15] proposed a blockchain-based peer-to-peer trading mechanism for electric vehicle aggregators, reducing intermediate losses by 3–5%. However, most existing studies focus on the scheduling optimization of electric vehicles as a single resource, neglecting their potential for coordination with thermal systems. Although the study [16] proposed an "electric vehicle-thermal storage" joint scheduling model, it treated thermal storage equipment as an independent heat source without considering the deep coupling of electricity–heat–hydrogen multi-energy flows, resulting in absorption capacity still being confined within the power system.

In terms of the wind–solar integration capacity of thermal energy storage in the electro–olefin–hydrogen electromagnetic energy supply device (EHED), the electrothermal conversion efficiency of the electric cracking furnace reaches more than 95%, and the waste heat recovery efficiency of the thermal storage system exceeds 85%, with the overall energy efficiency 20% higher than that of traditional electric boilers [17]. The measured data in Reference [18] shows that for every 1 MWh of curtailed wind power consumed by the EHED, it can simultaneously generate 3.2 GJ of thermal energy and 0.12 kg of hydrogen, with comprehensive benefits 30% higher than pure electric heating. The hydrogen produced by the dry gas reforming process can be used for fuel cell vehicles or industrial hydrogen energy, forming a value-added chain of "curtailed wind-hydrogen production-heating". Reference [19] constructs a joint operation model of EHEDs and hydrogen refueling stations, and subsidizes the thermal storage cost through hydrogen sales revenue, shortening the system investment payback period to 5–7 years. The thermal storage tank capacity can reach the GWh level, and the charging and discharging power adjustment range is 20–100%, which can match the short-period fluctuations (such as minute-level pitch control) of wind–solar output [20]. Reference [21] incorporates EHEDs into the regional integrated energy system, and reduces the grid peak–valley difference by 15–20% through the strategy of "valley power thermal storage-peak power heating".

In summary, existing literature has conducted extensive research on technologies for integrating wind–solar energy using EVs and thermal storage electromagnetic energy supply devices, but none have considered the joint optimization of EVs and thermal storage EHEDs for wind–solar integration.

1.3. The Main Contribution of This Article

This paper first analyzes the feasibility of EVs and thermal storage EHEDs participating in scheduling and establishes a model for maximizing the revenue of dispatchable EVs within the scheduling period. Secondly, it constructs a joint optimization scheduling strategy for wind–solar farms, EVs, thermal storage EHEDs, and the power grid. Then, considering the joint optimization scheduling of EVs and the thermal storage EHED, it establishes an objective function to minimize the system operation cost within the scheduling period, and solves the model using the CPLEX solver. Finally, the curtailment situation, EV revenue, and overall system operation cost under different scenarios are analyzed. The case study results verify the feasibility and superiority of the proposed model.

The main contributions of this paper are as follows:

(1) It proposes a joint optimization scheduling framework for electric vehicles (EVs) and thermal storage electro–olefin–hydrogen electromagnetic energy supply devices (EHEDs). Through the flexible charging/discharging of EVs and the collaborative operation of thermal storage/discharging of EHEDs, a hierarchical control strategy is designed to break through the limitation of single-device wind–solar integration.

(2) Develops a mixed-integer programming optimization framework adapted to the joint optimization scheduling framework, establishes the relationship between 0 and 1 variables and constraints such as coupled power balance and device operation boundaries, and realizes the collaborative optimization of wind–solar integration and economic operation through CPLEX solution, verifying the engineering practicability of the multi-energy complementary system.

(3) Based on the differentiated charging needs of vehicle owners, EVs are divided into three categories: “time-sensitive”, “price-sensitive”, and “revenue-seeking”. The potential of “price-sensitive” and “revenue-seeking” dispatchable EVs is focused on, and a dynamic electricity price incentive and battery loss cost compensation mechanism are proposed, significantly improving user participation willingness and deep wind–solar integration.

The structure and organization of this article are as follows: Section 2 analyzes the feasibility of scheduling electric vehicles and ethylene hydrogen equipment; the Section 3 proposes a joint optimization method; Sections 4 and 5 introduce cases and results; and the Section 6 summarizes the conclusion.

2. Feasibility Analysis of Electric Vehicles—Thermal Storage Electric–Olefin–Hydrogen Electromagnetic Power Supply Equipment

2.1. Classification and Model of Electric Vehicle Scheduling Potential

Electric vehicles, as a means of transportation, must first meet driving demands for grid-connected charging power. In practical scenarios, the demands of different EV owners for charging and “reverse charging” methods exhibit significant differences, i.e., the feasibility of participating in scheduling varies, whereas traditional charging methods do not consider the differentiated needs of EV owners. Therefore, this section classifies EV owners’ expected grid-connected charging power characteristics into three different types of charging and “reverse charging” modes based on their preferences.

(1) Time-sensitive: EV owners aim to achieve the desired charging power in the shortest time.
(2) Price-sensitive: EV owners expect to obtain power at the optimal price during grid-connected charging periods, ensuring the desired charging power before departure while avoiding battery degradation caused by "reverse charging".
(3) Revenue-seeking: EV owners aim to obtain power at the optimal price during grid-connected charging periods, while leveraging the "reverse charging" function to gain profits, ensuring the desired charging power before departure.

Based on the above three types of "charging" and "reverse charging" modes, the "time-sensitive" mode always meets EV charging demands with maximum charging power until the desired power is reached, lacking schedulability. The "price-sensitive" mode can consume curtailed wind and solar power at differentiated charging prices within specific periods, possessing schedulability. The "revenue-seeking" mode can consume curtailed wind and solar power at differentiated charging prices within specific periods and leverage the battery energy storage for "reverse charging", also possessing schedulability.

Classification and Model of Electric Vehicle Scheduling Potential

The "price-sensitive" and "revenue-seeking" charging modes can approximate the savings from differentiated charging prices as profits. Considering the battery degradation cost of the "reverse charging" mode in the "revenue-seeking" type, this paper aims to maximize the revenue of dispatchable EVs within a scheduling period, expressed as

$$C = \max(C_1 + C_2) \tag{1}$$

where C is the maximum revenue of EVs; C_1 is the revenue from the "price-sensitive" charging mode; and C_2 is the revenue from the "revenue-seeking" charging/discharging mode.

The revenue from the "price-sensitive" charging mode is expressed as

$$C_1 = \sum_{t=1}^{T} \sum_{i=1}^{N_Y} (\gamma_1 - \gamma_2) P_{Y,i}^t \tag{2}$$

where $P_{Y,i}^t$ is the charging power of "price-sensitive" EV i at time t; γ_1 and γ_2 are the original and preferential charging prices of EVs, respectively; N_Y is the number of EVs participating in the "price-sensitive" charging mode; and T is a scheduling period, T = 24.

The revenue from the "revenue-seeking" charging mode is expressed as

$$C_2 = \sum_{t}^{T} \sum_{i}^{N_H} \left[(\gamma_1 - \gamma_2) P_{H,i}^t + (\alpha_i - \beta_i) F_{H,i}^t \right] \tag{3}$$

where $P_{H,i}^t$ and $F_{H,i}^t$ are the charging power and "reverse charging" power of "revenue-seeking" EV i at time t, respectively, and α_i and β_i are the "reverse charging" price and battery degradation cost coefficient of EVs, respectively, with the stipulation that $\alpha_i > \beta_i$; N_H is the number of EVs participating in the "revenue-seeking" charging mode

$$\begin{cases} 0 \le P_{Y,i}^t \le P_{Y,i}^{rms} \\ 0 \le P_{H,i}^t \le P_{H,i}^{rms} \\ 0 \le F_{H,i}^t \le P_{H,i}^{rms} \end{cases} \tag{4}$$

where $P_{Y,i}^{rms}$ and $P_{H,i}^{rms}$ are the rated powers of "price-sensitive" and "revenue-seeking" EV i, respectively.

2.2. Energy Balance and Revenue Model of EHCD Equipment

The thermal energy storage electro–olefin–hydrogen device (TES-EHED) drives hydrocarbon steam cracking through electric energy (electric cracking furnace) and utilizes a thermal storage system to recover waste heat from the cracking process, improving energy efficiency. The system integrates wind–solar energy, thermal storage, hydrogen production, and EV charging modules, with the architecture shown in Figure 1:

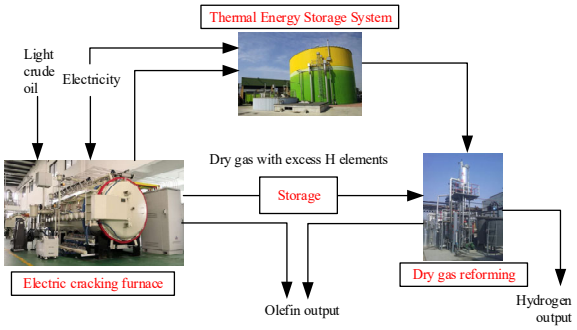


Figure 1. Architecture of thermal energy storage electro–olefin–hydrogen-EV joint system.

The core process is divided into three steps. First, light crude oil is input into the electric cracking furnace, where electromagnetic heating replaces the fuel furnace to crack light oil products into olefins such as ethylene and propylene, as well as hydrogen-rich dry gases like CH_4/C_2H_4. Second, waste heat from cracking furnace flue gas with a temperature exceeding 600 °C is recovered into the thermal storage system, stored by molten salt phase change materials to assist in hydrogen production. Finally, waste heat is used for dry gas reforming, i.e., hydrogen-rich dry gas is reformed to generate synthesis gas H_2 and olefins, further increasing hydrogen production.

2.2.1. Energy Balance Equation of Electro–Olefin–Hydrogen Device Cracking

$$\begin{cases} P_{EHCD} = Q_{Cracking} + Q_{Waste} \\ Q_{Cracking} = m_{raw} \cdot \Delta H_{Cracking} \\ Q_{Waste} = \eta_{Restore} \cdot (1 - \eta_{E2H}) \cdot P_{EHCD} \\ Q_{Waste} = Q_{waste} + Q_{waste\prime} \end{cases} \tag{5}$$

where P_{EHCD} is the input power of the EHED electric cracking furnace; $Q_{Cracking}$ is the heat absorbed by hydrocarbon cracking reaction; Q_{Waste} is the recoverable waste heat in cracking furnace flue gas; $\eta_{Restore}$ is the waste heat recovery efficiency of the thermal storage system; η_{E2H} is the electrothermal conversion efficiency; m_{raw} is the mass flow rate of light crude oil; $\Delta H_{Cracking}$ is the unit mass heat absorption of the cracking reaction; Q_{waste} is the waste heat absorbed by the thermal storage tank; and $Q_{waste\prime}$ is the heat loss during transmission to the thermal storage tank.

2.2.2. Thermal Storage Capacity and Heat Release Power

$$\begin{cases} Q_{store}(t) = \int_{t_0}^{t} (Q_{waste}(t) - Q_{release}(t))dt \\ Q_{release}(t) = Q_{H_2}(t) + Q_{H_2\prime}(t) + \alpha \cdot Q_{store}(t) \\ Q_{H_2}(t) = m_{H_2} \cdot \Delta H_{H_2} \end{cases} \tag{6}$$

where Q_{store} is the heat stored in the EHED thermal storage tank; $Q_{release}$ is the heat released by the thermal storage tank; Q_{H_2} is the heat demand for EHED dry gas reforming; $Q_{H_2\prime}$ is the heat loss during demand transmission; α is the heat loss coefficient; m_{H_2} is the mass flow rate of dry gas; and ΔH_{H_2} is the unit mass heat absorption of dry gas reforming.

2.2.3. Product Yield Model

$$\begin{cases} M_{drygas} = m_{raw} \cdot Y_{drygas} \cdot \Delta H_{Cracking} \\ M_{H_2} = m_{drygas} \cdot Y_{H_2} \cdot \Delta H_{H_2} \end{cases} \tag{7}$$

$$\begin{cases} Y_{drygas} = 0.25 X_{trans} \\ Y_{H_2} = 0.12 X_{trans} \end{cases} \tag{8}$$

$$\begin{cases} X_{trans} = 1 - e^{-k \cdot t} \\ k = 10^6 \cdot e^{-15000/T} \end{cases} \tag{9}$$

where M_{drygas} is the mass of generated dry gas (CH_4, C_2H_4, etc.); M_{H_2} is the mass of H_2 generated after dry gas reforming; Y_{drygas} is the mass yield of dry gas, i.e., the percentage of dry gas mass to raw material mass; Y_{H_2} is the mass yield of H_2 generated after dry gas reforming; X_{trans} is the single-pass conversion rate of raw materials, representing the decomposition proportion of raw materials in the cracking reaction; k is the cracking reaction rate constant, related to temperature; and T is the reaction residence time.

2.2.4. Dry Gas and Hydrogen Sales Revenue Model

The dry gas and hydrogen produced by the EHED device are sold in the market, and their sales revenues are as follows:

$$\begin{cases} R_{drygas} = M_{drygas} \cdot p_{drygas} \\ R_{H_2} = M_{H_2} \cdot p_{H_2} \end{cases} \tag{10}$$

where R_{drygas} and R_{H_2} are the sales revenues of dry gas and hydrogen, respectively, and p_{drygas} and p_{H_2} are the sales prices of dry gas and hydrogen, respectively.

3. Wind–Solar Collaborative Clustering Method Based on Improved K-Means++

This paper defines the pre-scheduled output of wind–solar energy by the power grid as primary wind–solar integration, and the positive difference between the theoretical wind–solar output and the pre-scheduled output as deep wind–solar integration. Figure 2 shows a schematic diagram of deep integration taking wind power as an example:

$$E_{deep} = \sum_{i=1}^{n} \left(\int_0^{t_1} Q_{deep,i,t} dt + \int_{t_2}^{t_3} Q_{deep,i,t} dt \right) \tag{11}$$

where t_1, t_2, and t_3 are the moments when the difference between the theoretical wind power output and the pre-scheduled output is zero.

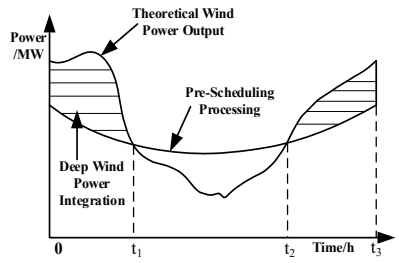


Figure 2. Schematic diagram of deep wind power integration.

This paper promotes deep wind–solar integration through the joint optimization of dispatchable electric vehicles (EVs) and thermal energy storage electro–olefin–hydrogen

electromagnetic energy supply devices (TES-EHEDs). The system architecture model is shown in Figure 3:

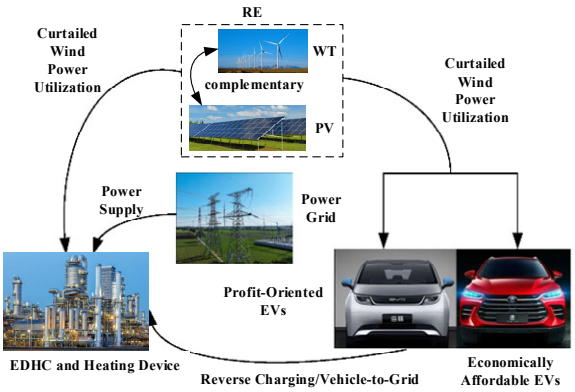


Figure 3. System architecture model.

Considering the deep wind–solar integration power, heating load, and configuration of dispatchable EVs, a joint optimization control strategy for dispatchable EVs-TES-EHEDs is proposed, as shown in Figure 4:

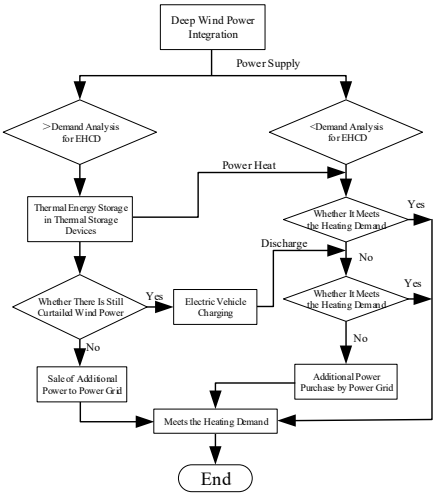


Figure 4. Joint optimization control strategy.

The specific joint optimization control strategy for dispatchable EVs-TES-EHEDs is as follows: when the difference between the theoretical wind–solar output and the pre-scheduled output is positive (i.e., deep wind–solar integration exists), the TES-EHED uses the deep integration part for heating. If the secondary wind–solar power exceeds the heating demand of TES-EHEDs, the remaining wind–solar energy is stored in the thermal storage device. If curtailed wind–solar power still exists, the two types of EVs ("price-sensitive" and "revenue-seeking") are scheduled to store the curtailed energy. When the secondary wind–solar power is less than the heating demand of the TES-EHED, the thermal storage device is used for heating. If the heating demand is satisfied, heating continues in this mode; if not, "revenue-seeking" EVs are scheduled to provide power support for TES-EHEDs through "reverse charging". If the heating demand is satisfied, maintain this mode; if not, purchase additional power from the grid to support TES-EHED heating. This strategy not only achieves deep wind–solar integration and reduces curtailment but also realizes peak shaving and valley filling.

3.1. Data Preprocessing

Data preprocessing is a fundamental step in ensuring the accuracy of subsequent analyses. This study employs linear interpolation to fill minor missing data, removes outliers beyond three standard deviations from the mean based on the 3σ principle, and finally maps data to the [0, 1] interval using min-max normalization. The normalization formula is

$$x' = \frac{x - x_{\min}}{x_{\max} - x_{\min}} \tag{12}$$

where x is the original feature value, $x_{\min}$ and $x_{\max}$ are the minimum and maximum values of the feature, respectively, and x' is the normalized feature value.

3.2. Feature Extraction

For wind turbine data, key features include wind speed change trends, power fluctuation amplitude, and wind direction periodicity. For photovoltaic data, features such as daily solar irradiance curves, temperature–power correlation, and peak power occurrence time are extracted. These features are obtained via mathematical statistics or curve fitting. For example, the power fluctuation amplitude is calculated as

$$\Delta P = P_{\max} - P_{\min} \tag{13}$$

where ΔP is the power fluctuation amplitude, and $P_{\max}$ and $P_{\min}$ are the maximum and minimum power values, respectively.

3.3. Dimensionality Reduction

Dimensionality reduction is performed using principal component analysis (PCA), which transforms the high-dimensional feature space into a low-dimensional principal component space via linear transformation, reducing computational complexity while retaining over 90% of the cumulative contribution rate. The core steps involve solving the eigenvalues and eigenvectors of the feature covariance matrix and selecting the eigenvectors corresponding to the top k largest eigenvalues to form the transformation matrix. Let the original feature vector be X, and the reduced-dimensional principal component vector be Y; the transformation formula is

$$Y = W^T \cdot X \tag{14}$$

where W is the transformation matrix composed of the eigenvectors of the first k principal components, and W^T is its transpose.

3.4. Improved K-Means++ Algorithm

The improved K-means++ algorithm introduces weight coefficients on the basis of the traditional algorithm to adjust the influence of wind turbine and photovoltaic features. Weight coefficients are determined according to the sample size ratio of the two energy sources, calculated as

$$w_i = \frac{n_i}{\sum_{j=1}^{2} n_j} \tag{15}$$

where w_i is the weight coefficient of the i-th energy source data (i = 1 for wind turbine data and i = 2 for photovoltaic data), n_i is the sample size of the i-th data, and $\sum_{j=1}^{2} n_j$ is the total sample size of the two types of data.

During clustering, the distance from a sample to a cluster center is calculated using weighted Euclidean distance, given by

$$d(x,c) = \sqrt{\sum_{k=1}^{m} w_k (x_k - c_k)^2} \tag{16}$$

where $d(x,c)$ is the weighted Euclidean distance from sample x to cluster center c, m is the feature dimension, x_k and ck are the k-th feature values of sample x and cluster center c, respectively, and w_k is the weight coefficient of the k-th feature.

4. Joint Optimization Scheduling of Electric Vehicles-Thermal Energy Storage Electro–Olefin–Hydrogen Device for Enhancing Deep Wind–Solar Integration

4.1. Objective Function

The optimization model aims to minimize the operation cost within the scheduling period, expressed as

$$F = min(F_1 + F_2 + F_3 + F_4 + F_5 + F_6 - R_7) \tag{17}$$

where F is the minimum operation cost; F_1 is the depreciation cost of thermal energy storage electro–olefin–hydrogen electromagnetic energy supply devices (TES-EHEDs); F_2 is the battery degradation cost from EV "reverse charging"; F_3 is the wind turbine generation cost; F_4 is the photovoltaic generation cost; F_5 is the joint scheduling cost; F_6 is the cost of additional power purchased from the grid; and R_7 is the sales revenue of dry gas and hydrogen.

4.1.1. Depreciation Cost of TES-EHED

Considering the depreciation cost of TES-EHED participating in deep wind–solar integration for heating, F_1 is expressed as

$$F_1 = \frac{V_r(1+V_r)^n}{(1+V_r)^n - 1}(\varphi_r P_r^{max} + \varphi_{eb} P_{eb}^{max}) / T_{yong} \tag{18}$$

where V_r is the annual discount rate of TES-EHEDs; n is the service life; φ_r and φ_{eb} are the investment costs of the thermal storage device and EHED, respectively; P_r^{max} and P_{eb}^{max} are the maximum powers of the thermal storage device and EHED, respectively; and T_{yong} is the usage duration within the scheduling period.

4.1.2. Battery Degradation Cost

The degradation cost of "revenue-seeking" EVs participating in deep wind–solar integration for heating, F_2, is expressed as

$$F_2 = \sum_{t=1}^{T} \sum_{i}^{N_H} \beta_i F_{H,i}^t \tag{19}$$

4.1.3. Wind Turbine Generation Cost

This paper only considers wind power participating in heating and dispatchable EV charging during deep integration periods, so F_3 is expressed as

$$F_3 = \sum_{t=0}^{t_1} \varepsilon_w P_w^{t,forecast} + \sum_{t=t_2}^{t_3} \varepsilon_w P_w^{t,forecast} \tag{20}$$

where $P_w^{t,forecast}$ is the theoretical wind power output at time t and ε_w is the unit generation cost coefficient of wind turbines.

4.1.4. Photovoltaic Generation Cost

The photovoltaic generation cost model F_4 comprehensively considers core factors such as initial investment, operation and maintenance costs, equipment life, and power generation, expressed as

$$F_4 = \frac{\sum_{h=1}^{24}\left[\left(\frac{I \cdot r \cdot (1+r)^n}{(1+r)^n - 1} + \frac{O_d}{24}\right) + S_h + L_h\right]}{\sum_{h=1}^{24} E_h \cdot \eta_h \cdot (1-\lambda_h)} \tag{21}$$

where I is the initial investment in photovoltaic installation; r is the discount rate; n is the equipment life period; O_d is the daily operation and maintenance cost; S_h is the scheduling service fee for the h-th hour; L_h is the energy storage loss cost for the h-th hour; E_h is the theoretical power generation for the h-th hour; η_h is the equipment efficiency for the h-th hour; and λ_h is the line loss rate for the h-th hour.

4.1.5. Joint Scheduling Cost

The joint scheduling cost function is set as

$$F_5 = \sum_{t=1}^{T}\left[\begin{array}{l} C_{curtailment} \cdot \left(P_{deep}(t) - P_{EHCD}(t) - P_{EV}(t)\right)^+ \\ +C_{gas} \cdot \left(D_{gas}(t) - S_{gas}(t)\right) \end{array}\right] \tag{22}$$

where $C_{curtailment}$ is the wind curtailment penalty coefficient; P_{deep} is the deep wind–solar integration power; C_{gas} is the penalty coefficient for gas supply–demand imbalance; $D_{gas}(t)$ is the gas demand at time t; and $S_{gas}(t)$ is the gas storage in the tank at time t.

The wind curtailment penalty coefficient $C_{curtailment}$ is expressed as

$$C_{curtailment} = \left[\begin{array}{l} \sum_{t=0}^{t_1} \partial_w \left(P_w^{t,forecast} - P_{w,e}^t\right) \\ + \sum_{t=t_2}^{t_3} \partial_w (P_w^{t,forecast} - P_{w,e}^t) \end{array}\right] \tag{23}$$

where $P_{w,e}^t$ is the wind–solar power fed into the grid at time t and ∂_w is the wind curtailment penalty conversion coefficient.

4.1.6. Cost of Additional Grid Power Purchase

As shown in the joint optimization control strategy (Figure 4), if TES-EHED, thermal storage, and "revenue-seeking" EVs meet the thermal power balance, no additional grid power is needed; otherwise, F_6 is expressed as

$$F_6 = \sum_{t=1}^{T} \pi_e^t P_{ec}^t \tag{24}$$

where P_{ec}^t is the additional grid power purchased and π_e^t is the grid electricity price.

4.1.7. Dry Gas and Hydrogen Sales Revenue

The total sales revenue from dry gas and hydrogen produced by TES-EHEDs through dry gas generation and reforming processes is

$$R_7 = R_{drygas} + R_{H_2} \tag{25}$$

4.2. Constraint Conditions

4.2.1. Power Balance Constraints

The electric power balance constraint is

$$P_{deep}^{t} + P_{grid}^{t} + P_{EVs+}^{t} - P_{EVs-}^{t} = P_{EHCD}^{t} \tag{26}$$

where P_{grid}^{t} is the exchanged power with the grid; P_{EVs+}^{t} is the reverse charging power of EVs and P_{EVs-}^{t} is the charging power of EVs.

The thermal power balance constraint is

$$\rho_{EHCD} P_{EHCD}^{t} + H_{r,in}^{t} = H_{r,out}^{t} + H_{load}^{t} \tag{27}$$

where $H_{r,in}^{t}$ and $H_{r,out}^{t}$ are the heat storage and release powers of the thermal storage device at time t, respectively; H_{load}^{t} is the thermal load at time t; and ρ_{EHCD} is the electrothermal conversion efficiency of EHEDs, taken as 95%.

4.2.2. Deep Wind–Solar Integration Power Constraint

The joint integration power of EV-TES-EHEDs at time t, P_{deep}^{t}, shall not exceed the secondary wind–solar power P_{w}^{t}

$$\begin{cases} 0 \le P_{deep}^{t} \le P_{w}^{t} \\ P_{EHCD}(t) \le \eta_{E2H} \cdot P_{deep}(t) \end{cases} \tag{28}$$

4.2.3. Operation Constraints of TES-EHED

The EHED constraints are

$$0 \le P_{EHCD}^{t} \le P_{EHCD}^{max} \tag{29}$$

The thermal storage device constraints are

$$\begin{cases} S_{r}^{t} = S_{r}^{t-1} + (\omega_{r}^{t} \cdot H_{r,in}^{t} - (1 - \omega_{r}^{t}) \cdot H_{r,out}^{t}) \\ 0 \le S_{r}^{t} \le S_{r}^{max} \\ 0 \le H_{r,in}^{t} \le H_{r,in}^{max} \\ 0 \le H_{r,out}^{t} \le H_{r,out}^{max} \end{cases} \tag{30}$$

where S_{r}^{t} and S_{r}^{t-1} are the thermal storage capacities at times t and $t-1$, respectively; S_{r}^{max} is the maximum thermal storage capacity; $H_{r,in}^{max}$ and $H_{r,out}^{max}$ are the maximum heat storage and release powers, respectively; and ω_{r}^{t} is the charging/discharging state of the thermal storage device at time t (1 for storage, 0 for release).

Gas storage device constraints, the amount of gas in the tank is related to chemical gas demand:

$$S_{gas}(t+1) = S_{gas}(t) + Y_{gas} \cdot m_{raw} - D_{gas}(t) \tag{31}$$

4.3. Solution to Joint Optimization Model Based on Mixed-Integer Programming

Mathematically, the decision variables in the model include both continuous values (within upper and lower bounds of constraints) and integer values (e.g., 0–1 variables). Therefore, the established joint optimization economic dispatch model is a 0–1 mixed-integer linear programming (MILP) model, expressed as

$$\begin{cases} \min c_{t} \\ s.t., Ax = B \\ x_{min} \le x_{i} \le x_{max}, i \in I \\ x_{j} \in \{0,1\}, j \in I \end{cases} \tag{32}$$

where the optimization variables include EHED operation power, thermal storage charging/discharging power, and dispatchable EV charging/reverse charging power; equality constraints include electric power balance, thermal power balance, and thermal storage device constraints; and inequality constraints include deep wind–solar integration power constraints, EHED constraints, thermal storage device constraints, and dispatchable EV operation constraints. The model is solved using the CPLEX 20.1 solver in MATLAB R2022b based on mixed-integer linear programming.

5. Case Study

5.1. Case Description

The thermal storage device has a heat storage capacity of 300 MW, with an investment cost of 5×10^4 yuan/MW. The electro–olefin–hydrogen electromagnetic energy supply device (EHED) has an installed capacity of 200 MW, an investment cost of 1×10^6 yuan/MW, and a maximum heat storage/discharge capacity of 50 MW. The annual discount rate is 6%, and the service life is 20 years [21]. The maximum number of EVs that can be connected to the system is set to 6000. Table 1 lists the relevant parameters of EVs, and the number of EVs connected in each time period within a scheduling period is shown in Figure 5. The unit power supply price of the power grid refers to Reference [22], the charging price for conventional EVs and dispatchable EVs refers to Reference [23]. The "reverse charging" price for "revenue-seeking" EVs is defined as 20% higher than the charging price for dispatchable EVs [24], and the battery maintenance cost is defined as 5% of the "reverse charging" price [25]. The case study is a day-ahead dispatch with a scheduling period of 24 h, and the unit dispatch time Δ is 1 h [26,27].

Table 1. System thermal load power.

Time	EHED Load (MW)	Time	EHED Load (MW)
22	906.55	10	931.68
23	915.21	11	902.05
24	958.89	12	911.30
1	957.37	13	862.78
2	963.83	14	851.33
3	969.89	15	858.91
4	957.33	16	842.03
5	946.16	17	857.08
6	944.53	18	857.62
7	942.45	19	860.39
8	937.17	20	894.17
9	941.36	21	925.83

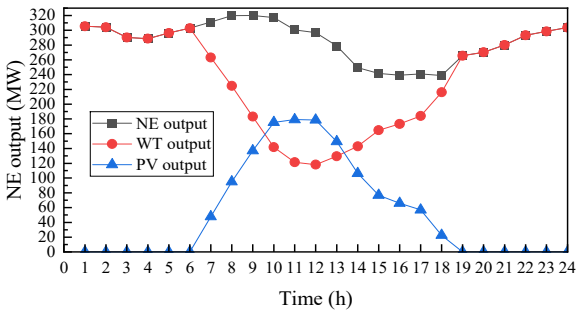


Figure 5. Theoretical output of new energy.

As shown in Figure 5, the theoretical output of wind–solar new energy with a 24 h scheduling period is obtained by the improved K-means++ algorithm.

5.2. Simulation Analysis

To compare and analyze the wind–solar integration, dispatchable EV revenue, and system operation cost before and after the joint optimization of EVs and thermal storage EHEDs, three different scenarios are set, where the EV demand response intention is "time-sensitive" [28–31].

Scenario 1: Power system with wind–solar energy considering only EVs;

Scenario 2: Power system with wind–solar energy considering only thermal storage EHEDs;

Scenario 3: Power system with wind–solar energy considering joint optimization of EVs and thermal storage EHEDs.

5.2.1. Deep Wind–Solar Integration Analysis

Figure 6 shows the comparative analysis of wind–solar integration under the three scenarios. As analyzed in Figure 6a, a large amount of wind curtailment occurs between 22:00 and 08:00 (curtailment period) because the electricity load is at a low level during this period, while wind power generation is high. Although EVs participate in scheduling to integrate wind curtailment, it is still insufficient to improve the curtailment situation significantly. During 09:00–21:00 (non-curtailment period), the electricity load increases, wind–solar power generation declines, and EVs participate in scheduling, alleviating wind curtailment. The curtailment situation in Figure 6b is similar to that in Figure 6a: during peak wind power periods, the self-integration capacity is insufficient, leading to significant curtailment; and during low wind power periods, the electricity load increases, and self-scheduling integrates part of the curtailment, improving the situation. Figure 6c shows that the joint optimization of EVs and thermal storage EHEDs to integrate wind curtailment significantly improves curtailment in both curtailment and non-curtailment periods.

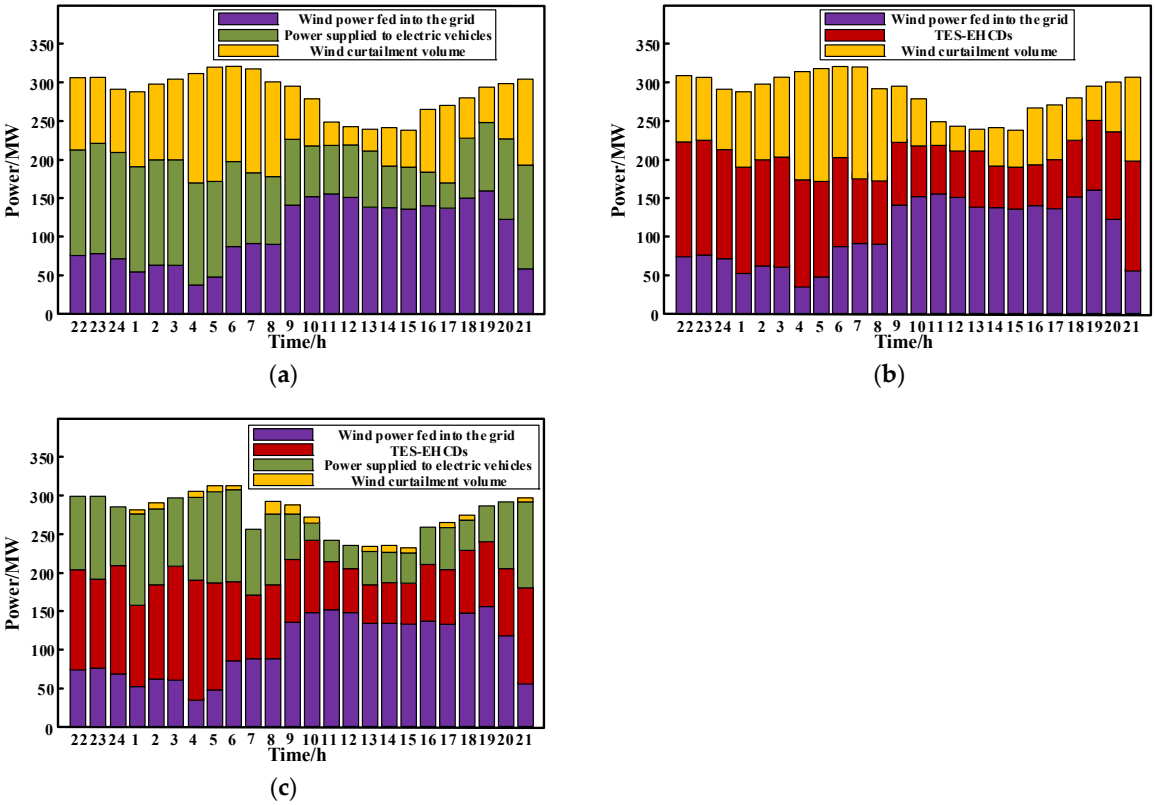


Figure 6. Analysis of wind–solar integration under three scenarios. (**a**) Wind–solar integration in Scenario 1; (**b**) wind–solar integration in Scenario 2; and (**c**) wind–solar integration in Scenario 3.

5.2.2. Comparison of System Operation Cost, EV Revenue, and Wind Curtailment Rate Under Three Scenarios

The economic dispatch results for the three scenarios, including system operation cost, EV revenue, and wind curtailment rate, are shown in Table 2.

Table 2. Comparison of operation cost, EV revenue, and wind–solar integration rate.

Scenario	Operation Cost (10^4 Yuan)	EV Cost (10^4 Yuan)	Wind Curtailment Power (MW)	Curtailment Rate (%)
Scenario 1	101.03	4.46	223.2	3.26
Scenario 2	97.16	/	215.64	3.15
Scenario 3	42.80	2.34	193.2	1.37

Overall, the system operation cost and curtailment rate of the two modes (Scenario 2 considering thermal storage EHEDs and Scenario 1 considering dispatchable EVs) for deep wind–solar integration are approximately the same. However, considering the joint optimization of dispatchable EVs and thermal storage EHEDs for wind–solar integration (Scenario 3), the system operation cost and curtailment rate significantly decrease. This is because the joint integration deeply utilizes wind–solar energy, with dispatchable EVs serving as a backup for EHEDs to further integrate remaining curtailed energy. The reduction in wind curtailment power leads to a decrease in operation cost. The EV revenue in Scenario 3 is higher than that in Scenario 1 because, in addition to dispatchable EVs participating in deep wind–solar integration at lower charging prices, "revenue-seeking" EVs in Scenario 3 participate in the "reverse charging" mode, further increasing revenue.

5.2.3. Joint Dispatch Optimization Under Different EV Demand Response Intentions

To further analyze and compare, three types of EV participation in "reverse charging" are set, corresponding to EV demand response degrees of "time-sensitive", "price-sensitive", and "revenue-seeking".

Scenario 3: Joint optimization of EVs and thermal storage EHEDs for wind–solar integration, with EV demand response degree set to "time-sensitive";

Scenario 4: Joint optimization of EVs and thermal storage EHEDs for wind–solar integration, with EV demand response degree set to "price-sensitive";

Scenario 5: Joint optimization of EVs and thermal storage EHEDs for wind–solar integration, with EV demand response degree set to "revenue-seeking".

Figure 7 shows the variation trend of theoretical power and integration rate under different scenarios:

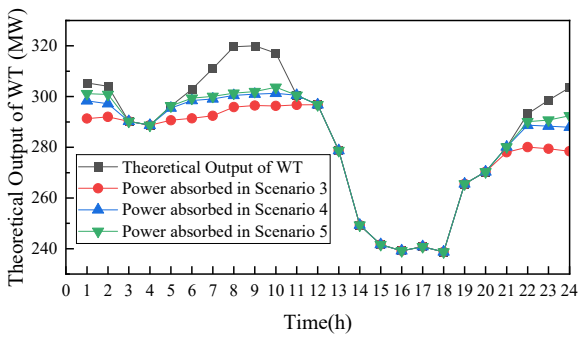


Figure 7. Comparison of daily curves of integrated power under different intentions.

In terms of wind–solar utilization indicators, the peak wind curtailment power in Scenario 3 drops to 25.14 MW, with an average of 8.05 MW; in Scenario 4, the peak curtailment

power is 19.19 MW and the average is 4.82 MW, a 40.12% decrease; and in Scenario 5, the peak curtailment power is only 18.29 MW and the average is 3.9 MW, a 19.09% decrease compared to Scenario 4.

The curtailment rates for each scenario were as follows: Scenario 3: 2.82%, Scenario 4: 1.69%, and Scenario 5: 1.37%, showing an approximately linear downward trend.

Table 3 compares the economic indicators under different scenarios:

Table 3. System operation cost and EV revenue analysis.

Scenario	Operation Cost (10^4 Yuan)	EV Revenue (10^4 Yuan)	EV Reverse Charging Revenue (10^4 Yuan)	Power Purchase Cost (10^4 Yuan)
Scenario 3	42.8	−2.341	/	16.93
Scenario 4	35.21	−0.727	/	9.72
Scenario 5	30.93	3.219	3.809	5.44

As the intention increases, EVs integrate more curtailed wind–solar energy, reducing grid power purchase demand. The system power purchase cost in Scenario 5 decreases by 67.87% and 44.03% compared to Scenarios 4 and 3, respectively. Meanwhile, the thermal storage utilization rate of EHEDs increases, and the equipment depreciation cost is allocated more efficiently.

The revenues of "time-sensitive" and "price-sensitive" EVs in the three scenarios are negative, meaning that in these two cases, EVs can only reduce energy costs through demand response. As the demand response degree increases to the "revenue-seeking" stage, the total EV revenue turns from loss to profit. In Scenario 5, reverse charging revenue accounts for 96.53%, becoming the main revenue source.

Figure 8 shows the power balance during the peak period from 21:00 to 06:00:

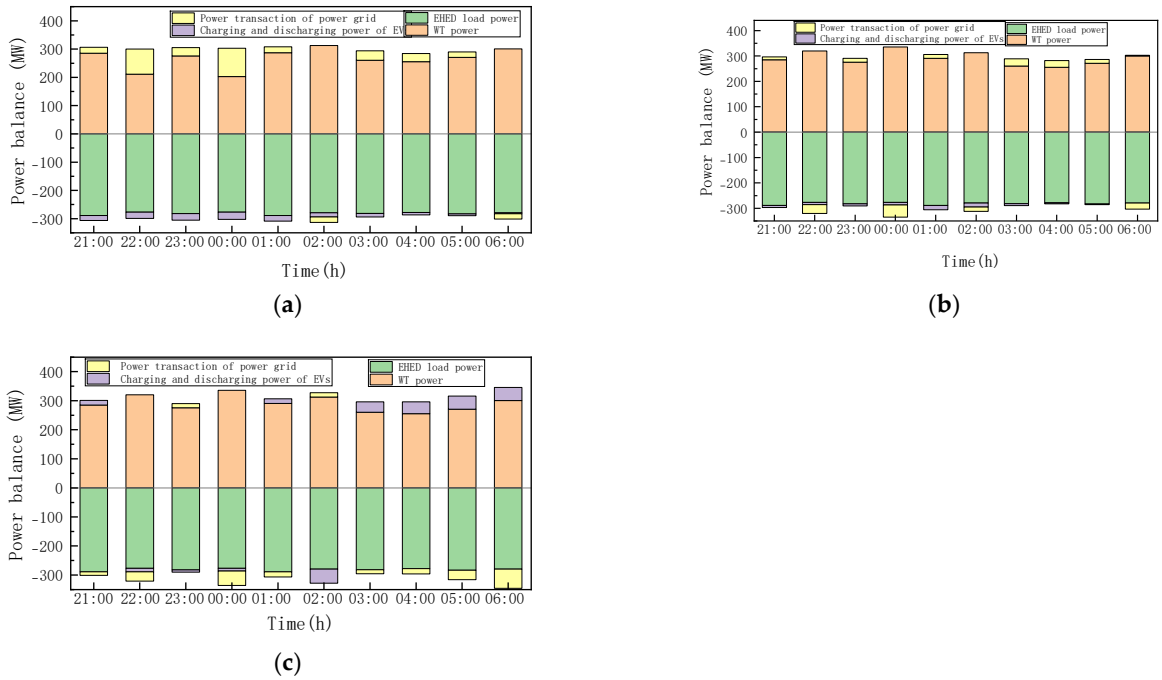


Figure 8. Comparison of power balance in typical periods. (**a**) Power balance in Scenario 4 peak period; (**b**) power balance in Scenario 5 peak period; and (**c**) power balance in Scenario 6 peak period.

The thermal load satisfaction rate reaches 100% in all scenarios, and the collaboration between EHED thermal storage and EV reverse charging ensures the heating reliability of dry gas generation. In Scenario 3, 100.24 MW of power needs to be purchased during peak periods. In Scenario 5, the maximum purchased power is only 14.92 MW through EV reverse charging and EHED thermal storage, and the total power fed back to the grid is as high as 213.14 MW, far higher than 10.98 MW in Scenario 4, further achieving "negative power purchase". Under high intention, EVs not only serve as "loads" but also become "flexible power sources", significantly reducing grid peak load pressure and improving system stability [28].

Figure 9 plots the cost and curtailment rate curves under different EV demand response intentions:

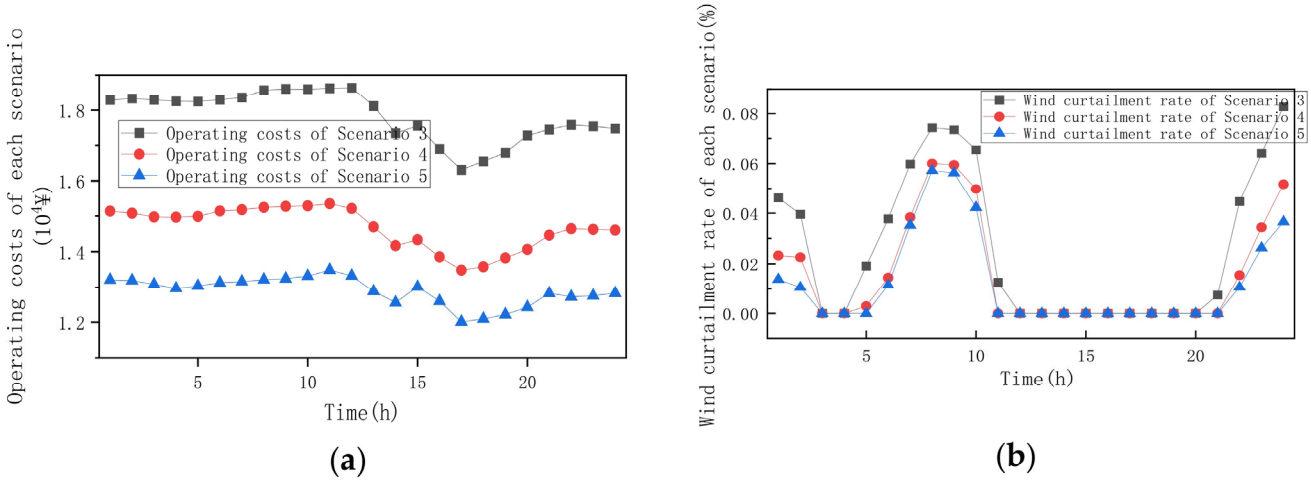


Figure 9. Cost and curtailment rate curves under different EV intentions. (**a**) Operation cost of each scenario and (**b**) curtailment rate of each scenario.

Under the "time-sensitive" intention of EV charging in Scenario 3, the curtailment rate and cost show a significant positive correlation, with costs increasing simultaneously during concentrated curtailment periods (1–2, 6–10, and 22–24 h). For example, at hour 8, the curtailment rate is 7.43%, and the cost is CNY 18,572, the highest of the day; from hours 13–20, the curtailment rate is 0%, and the cost drops to CNY 16,300–18,100, an 8.5–12.0% decrease from the peak period. This is because EVs only respond with "time-sensitive", having limited curtailment integration capacity, where curtailment penalties dominate cost fluctuations, and reverse charging revenue is absent, as the EV revenue in Table 3 for Scenario 3 is negative.

Under the "price-sensitive" intention of EV charging in Scenario 4, the curtailment rate significantly decreases. For example, at hour 8, the curtailment rate is 6.00%, a 19.2% decrease from Scenario 3, and the cost fluctuation range narrows. During the high curtailment period at hour 24, the curtailment rate is 5.17%, and the cost is only CNY 14,601, a 16.5% decrease from the same period in Scenario 3. This is because EVs are sensitive to prices, increasing charging during nighttime curtailment periods to integrate curtailment and reduce penalty costs; meanwhile, the charging cost of EVs under "price-sensitive" response in non-curtailment periods decreases, smoothing the daily cost curve.

Under the "reverse charging" intention of EV charging in Scenario 5, the curtailment rate further decreases. For example, at hour 8, the curtailment rate is 5.72%, but the cost and curtailment rate show a "deviation"—in some high curtailment periods, such as hour 7 with a curtailment rate of 3.53%, the cost is only CNY 13,161, lower than CNY 15,171 in the same period for Scenario 4. This is because EVs profit through "reverse charging",

accounting for 96.53% of total revenue. During high curtailment periods, EVs not only integrate curtailment to reduce penalties but also increase revenue through power sales, forming a dual effect of "cost reduction + revenue increase". For example, at hour 22 in Scenario 5, the curtailment rate is 1.06%, and the cost is CNY 12,724, a 27.6% decrease from the same period in Scenario 3 (curtailment rate 4.47%, cost CNY 17,582), with revenue exceeding the total EV revenue of CNY 32,190 in Scenario 5.

Therefore, when the intention increases from "time-sensitive" to "price-sensitive", the comprehensive curtailment rate decreases by 3.11%, and when increasing from "price-sensitive" to "revenue-seeking", the decrease narrows to 1.51%, indicating a "scale saturation effect", i.e., the curtailment rate is limited by the maximum number of EVs connected (6000). When the intention increases by 0.2 each time, the cost decreases by 17.7% and 12.16%, respectively, reflecting that reverse charging revenue gradually dominates as the scale expands, but user participation costs, such as battery degradation compensation, may limit further intention improvement.

6. Conclusions

This paper addresses the problem of long heating periods and severe wind curtailment during winter in northern China. It analyzes the feasibility of electric vehicles (EVs) participating in scheduling, proposes a joint optimization control strategy for dispatchable EVs and thermal energy storage electro–olefin–hydrogen electromagnetic energy supply devices (TES-EHEDs), and establishes an economic dispatch model targeting maximum revenue of dispatchable EVs and minimum system operation cost. Through case studies, the specific conclusions are as follows:

Effectiveness of Wind–Solar Integration. The collaborative operation of EVs and TES-EHEDs reduces the wind curtailment rate from 3% in traditional scenarios to 1.37%, with wind curtailment power decreasing by over 54%. This verifies the significant effect of the joint model on deep wind–solar integration.

Economic Benefits of Joint Scheduling. Compared with single-device scenarios, the system operation cost in the joint dispatch scenario is reduced by 57.63% to CNY 582,300. Meanwhile, "time-sensitive" EV users further reduce costs by 47.53% through adjusted power consumption patterns, forming a sustainable user incentive mechanism.

Robustness of the Energy System. The joint dispatch strategy prioritizes wind–solar energy for TES-EHEDs and uses EVs as backup. Under different EV demand response degrees ("time-sensitive", "price-sensitive", and "revenue-seeking"), it ensures thermal load demand while achieving "peak shaving and valley filling" for the power grid, reducing reliance on grid power purchase during peak periods, and enhancing energy system robustness.

In conclusion, the joint control strategy of dispatchable EVs and TES-EHEDs demonstrates superior performance in wind curtailment reduction compared with the independent dispatch of EVs or TES-EHEDs. It significantly reduces system operation costs and increases dispatchable EV revenue, providing a practical solution for the deep integration of wind–solar energy in northern heating areas.

Author Contributions: Date curation, Formal analysis, C.W. (Chenglong Wang); Conceptualization, Methodology, S.S.; Formal analysis, Visualization, N.W.; Investigation, Resources, S.W.; Software, Validation, Y.C.; Visualization, Data analysis, L.S.; Writing, X.L.; Formal analysis, Methodology, C.W. (Chengfu Wang); Methodology, Validation, G.Z. All authors have read and agreed to the published version of the manuscript.

Funding: This work is funded by State Grid Shandong Electric Power Company for Science and Technology Project: "Research on Load Characteristic Modeling of Electro—Olefin—Hydrogen Electromagnetic Energy Supply and Grid Interaction Technology" (Grant No. B30626240016).

Data Availability Statement: The original contributions presented in this study are included in the article. Further inquiries can be directed to the corresponding author.

Conflicts of Interest: Authors Shumin Sun, Chenglong Wang, Yan Cheng, Shibo Wang, Liqun Sun, Guangqi Zhou and Nan Wang were employed by Electric Power Research Institute of State Grid Shandong Electric Power Company. The remaining authors declare that the research was conducted in the absence of any commercial or financial relationships that could be construed as a potential conflict of interest. The authors declare that this study received funding from State Grid Shandong Electric Power Company. The funder had the following involvement with the study: methodological analysis and theoretical derivation.

References

1. Callaway, D.S. Tapping the energy storage potential in electric loads to deliver load following and regulation, with application to wind energy. *Energy Convers. Manag.* **2009**, *50*, 1389–1400. [CrossRef]
2. Baohong, J. Impact of renewable energy penetration in power systems on the optimization and operation of regional distributed energy systems. *Energy* **2023**, *273*, 127201. [CrossRef]
3. Aydin, E.; Iqbal, S. Reinforcement Learning-Based Optimization for Electric Vehicle Dispatch in Renewable Energy Integrated Power Systems. In Proceedings of the 2024 IEEE Energy Conversion Congress and Exposition (ECCE), Phoenix, AZ, USA, 20–24 October 2024; pp. 1297–1304.
4. Bojod, J.; Erkal, B. Distributed Energy Resources for Techno-Economic with Ant Colony Optimization (ACO) based Artificial Neural Network. In Proceedings of the 2024 7th International Conference on Energy, Electrical and Power Engineering (CEEPE), Yangzhou, China, 26–28 April 2024; pp. 1443–1448.
5. National Energy Administration. Notice on Issuing the Clean Heating Plan for Winter in Northern Regions (2017–2021) [EB/OL]. 27 December 2017. Available online: https://www.ndrc.gov.cn/xxgk/zcfb/tz/201712/t20171220_962623.html?code=&state=123 (accessed on 28 September 2025).
6. Ding, T.; Mu, C.; He, Y.; Sun, Y.; Liu, R.; He, F.; Ren, C. Analysis on Current Situation of Clean Heating Policies and Typical Cases in Northwest China (II): Typical Cases and Economic Analysis. *Proc. CSEE* **2020**, *40*, 5126–5136. [CrossRef]
7. Bojod, J.; Erkal, B. A New Approach in Distributed Energy Resources for Techno-Economic with Metaheuristic Method and Artificial Neural Network. In Proceedings of the 2023 IEEE International Conference on Integrated Circuits and Communication Systems (ICICACS), Raichur, India, 24–25 February 2023; pp. 1–6.
8. Chen, S.; Xin, H.; Wang, T.; Yang, J.; Peng, D.; Tan, Z. Robust Optimization Model for Joint Heating Dispatch of Wind Power and Thermal Storage Electric Boiler. *Electr. Power Constr.* **2016**, *37*, 103–109.
9. Li, Y.; Yu, C.; Liu, Y.; Ni, Z.; Ge, L.; Li, X. Collaborative Operation Between Power Network and Hydrogen Fueling Stations with Peer-to-Peer Energy Trading. *IEEE Trans. Transp. Electrif.* **2023**, *9*, 1521–1540. [CrossRef]
10. Jin, C.; Tang, J.; Ghosh, P. Optimizing Electric Vehicle Charging: A Customer's Perspective. *IEEE Trans. Veh. Technol.* **2013**, *62*, 2919–2927. [CrossRef]
11. Yadav, K.; Singh, M. Dynamic scheduling of electricity demand for decentralized EV charging systems. *Sustain. Energy Grids Netw.* **2024**, *39*, 101467. [CrossRef]
12. Panda, S.; Ganguly, S. Multi-objective smart charging scheduling scheme for EV integration and energy loss minimization in active distribution networks using mixed integer programming. *Sustain. Energy Grids Netw.* **2025**, *43*, 101743. [CrossRef]
13. Zhang, C.; Yin, W.; Wen, T. An advanced multi-objective collaborative scheduling strategy for large scale EV charging and discharging connected to the predictable wind power grid. *Energy* **2024**, *287*, 129495. [CrossRef]
14. Wang, H.; Wang, Y.; Bian, J.; Li, G.; Meng, X. A Two-Layer Real-Time Dispatch Strategy for Large-Scale Electric Vehicles Connected to Power Grid Based on Improved Rolling Horizon Method. *Power Syst. Technol.* **2025**. [CrossRef]
15. Yoon, S.-G.; Choi, Y.-J.; Park, J.-K.; Bahk, S. Stackelberg-game-based demand response for at-home electric vehicle charging. *IEEE Trans. Veh. Technol.* **2016**, *65*, 4172–4184. [CrossRef]
16. Hakimi, S.M.; Hasankhani, A.; Shafie-khah, M.; Catalão, J.P.S. Stochastic planning of a multi-microgrid considering integration of renewable energy resources and real-time electricity market. *Appl. Energy* **2021**, *298*, 117215. [CrossRef]
17. Amirioun, M.H.; Jafarpour, S.; Abdali, A.; Guerrero, J.M.; Khan, B. Resilience-Oriented Scheduling of Shared Autonomous Electric Vehicles: A Cooperation Framework for Electrical Distribution Networks and Transportation Sector. *J. Adv. Transp.* **2023**, *2023*, 7291712. [CrossRef]

18. Hu, A.; Zhang, T.; Li, G.; Cheng, W.; Wang, J. Cloud-Edge Collaborative Scheduling Method for Virtual Power Plant Considering Parameter Consistency of Electric Vehicles. *Autom. Electr. Power Syst.* **2025**, *49*.
19. Khan, R.; Mehmood, K.K.; Bukhari, S.B.A.; Imran, K.; Wadood, A.; Rhee, S.B.; Park, S. An Optimization-Based Reliability Enhancement Scheme for Active Distribution Systems Utilizing Electric Vehicles. *IEEE Access* **2021**, *9*, 157247–157258. [CrossRef]
20. Marasciuolo, F.; Orozco, C.; Dicorato, M.; Borghetti, A.; Forte, G. Chance-Constrained Calculation of the Reserve Service Provided by EV Charging Station Clusters in Energy Communities. *IEEE Trans. Ind. Appl.* **2023**, *59*, 4700–4709. [CrossRef]
21. Dalala, Z.; Al-Omari, M.; Al-Addous, M.; Bdour, M.; Al-Khasawneh, Y.; Alkasrawi, M. Increased renewable energy penetration in national electrical grids constraints and solutions. *Energy* **2022**, *246*, 123361. [CrossRef]
22. Motlagh, S.G.; Oladigbolu, J.; Li, L. A review on electric vehicle charging station operation considering market dynamics and grid interaction. *Appl. Energy* **2025**, *392*, 126058. [CrossRef]
23. Mediwaththe, C.P.; Smith, D.B. Game-theoretic electric vehicle charging management resilient to non-ideal user behavior. *IEEE Trans. Intell. Transp. Syst.* **2018**, *19*, 3486–3495. [CrossRef]
24. Neaimeh, M.; Wardle, R.; Jenkins, A.M.; Yi, J.; Hill, G.; Lyons, P.F.; Hübner, Y.; Blythe, P.T.; Taylor, P.C. A probabilistic approach to combining smart meter and electric vehicle charging data to investigate distribution network impacts. *Appl. Energy* **2015**, *157*, 688–698. [CrossRef]
25. Wang, S.Y.; Yu, J.L. Optimal sizing of the CAES system in a power system with high wind power penetration. *Int. J. Electr. Power Energy Syst.* **2012**, *37*, 117–125. [CrossRef]
26. Ren, L.; Yuan, M.; Jiao, X. Electric vehicle charging and discharging scheduling strategy based on dynamic electricity price. *Eng. Appl. Artif. Intell.* **2023**, *123*, 106320. [CrossRef]
27. Sun, S.; Yang, Q.; Yan, W. Optimal temporal-spatial electric vehicle charging demand scheduling considering transportation-power grid couplings. In Proceedings of the 2018 IEEE Power & Energy Society General Meeting, PESGM, Portland, OR, USA, 5–10 August 2018; IEEE: Piscataway, NJ, USA, 2018; pp. 1–5.
28. Fang, C.; Lu, H.; Hong, Y.; Liu, S.; Chang, J. Dynamic pricing for electric vehicle extreme fast charging. *IEEE Trans. Intell. Transp. Syst.* **2021**, *22*, 531–541. [CrossRef]
29. Zhou, B.; Yao, F.; Littler, T.; Zhang, H. An electric vehicle dispatch module for demand-side energy participation. *Appl. Energy* **2016**, *177*, 464–474. [CrossRef]
30. Xu, H.; Yu, C.; Chen, C.; Guo, L.; Su, J.; Li, M.; Zhang, X. Impedance model-based stability analysis of single-stage grid-connected inverters considering PV panel characteristics and DC-side voltage. *Prot. Control Mod. Power Syst.* **2025**, *10*, 130–145. [CrossRef]
31. Qiu, J.; Du, L. Optimal dispatching of electric vehicles for providing charging on-demand service leveraging charging-on-the-move technology. *Transp. Res. Part C Emerg. Technol.* **2023**, *146*, 103968. [CrossRef]

Disclaimer/Publisher's Note: The statements, opinions and data contained in all publications are solely those of the individual author(s) and contributor(s) and not of MDPI and/or the editor(s). MDPI and/or the editor(s) disclaim responsibility for any injury to people or property resulting from any ideas, methods, instructions or products referred to in the content.